Biosensors and Bioelectronics 171 (2021) 112690

Contents lists available at ScienceDirect

Biosensors and Bioelectronics

journal homepage: http://www.elsevier.com/locate/bios

Encapsulating enzyme into metal-organic framework during in-situ growth on cellulose acetate nanofibers as self-powered glucose biosensor

Xin Li [a], Quan Feng [c], Keyu Lu [d], Jieyu Huang [a], Yanan Zhang [a], Yutong Hou [a], Hui Qiao [a], Dawei Li [b,*], Qufu Wei [a,**]

[a] Key Laboratory of Eco-Textiles, Ministry of Education, Jiangnan University, 1800 Lihu Avenue, Wuxi, Jiangsu Province, 214122, PR China
[b] College of Textile and Clothing, Nantong University, Nantong, Jiangsu 226019, PR China
[c] Key Laboratory of Textile Fabric, Anhui Polytechnic University, Wuhu, Anhui, 241000, PR China
[d] State Key Laboratory of Food Science and Technology, Jiangnan University, 1800 Lihu Avenue, Wuxi, Jiangsu Province, 214122, PR China

ARTICLE INFO

Keywords:
Enzymatic biofuel cells
Glucose biosensor
Metal-organic frameworks
Cellulose acetate
Long-term monitoring

ABSTRACT

Development of reliable Enzymatic Biofuel Cells (EBFC)-based self-powered glucose biosensor for continuous, noninvasive monitoring without restriction on patient's movement is highly recommendable. However, its application to a large extent is limited by the relatively poor stability. Herein, we synthesized a highly flexible electrode for effective enzyme immobilization by encapsulating enzyme into the metal-organic frameworks (MOFs) and robustly anchored to the cellulose acetate (CA) nanofiber membrane. As is well-known, such nanostructured fiber materials are the first time to be synthesized for glucose biosensor, which encapsulated biomolecules in MOFs platform during the MOFs in-situ growth on the nanofiber membranes. The as-proposed biosensor demonstrated excellent stability over 15 h of continuous long-term monitoring. The remarkable stability of assembled self-powered glucose biosensor in this work could inspire the application of enzymatic biosensors in biometrics, chronic disease management and clinical diagnosis.

1. Introduction

The glucose level in blood is a critical technical indicator due to glucose as an essential energy source for cellular activity in the living body can closely affect the physiological homeostasis system of the human body (Lee et al., 2018). However, a mass of people suffer from diabetes caused by metabolic disorder involving glucose processing, which is also one of the most extensive chronic diseases caused by the dysfunction of insulin secretion (Gao et al., 2016). More seriously, excess glucose in the blood plasma leads to complications such as blindness, cardiovascular disease and kidney failure (Lipani et al., 2018). Therefore, it is very urgent to monitor and control blood glucose levels (Lin et al., 2019a). Electrochemical analysis becomes an ideal explore by many researchers due to its selectivity (Park et al., 2018), sensitivity (Kwon et al., 2019) and miniaturization (Barton et al., 2004), additionally, electrochemical sensor can transform analytical substrates into electrical signals through oxidation-reduction reactions, which have been achieved for protein (Chen et al., 2019), heavy metal ions (Nyein et al., 2016) and other biomarkers of exploration (Sakthivel et al., 2019). As a novel electrochemical sensor (Xu et al., 2010), EBFC-based self-powered biosensor with advantages of low cost (Wang et al., 2018), anti-interference (Katz et al., 2001) and no need for extra power supply (Miyake et al., 2011), has attracted considerable attention in recent years and has been already successfully utilized in various biomarkers (Fan et al., 2020). Sun. et al. prepared a EBFC-based sensor for formaldehyde detection (Sun et al., 2019a). Lv. et al. reported a self-powered sensor for glucose detection by conductive bacterial cellulose (Lv et al., 2018). We established a self-powered sensing platform for bisphenol A detection (Li et al., 2020a). However, the long-term working stability of the self-powered biosensor is still a challenge due to the core position of the enzyme in the device (Yang and Gao, 2019).

Enzymes are key biomolecules capable of effectively catalyzing life-sustaining biological conversion in complex ecosystems (Chen et al., 2020). Inspired by their outstanding specificity and selectivity (Mahmoodi and Saffar-Dastgerdi, 2020), increasing efforts are devoted to apply enzymatic transformations in vivo to sensing devices as signal

* Corresponding author.
** Corresponding author.
E-mail addresses: dawei1026@jiangnan.edu.cn (D. Li), qfwei@jiangnan.edu.cn (Q. Wei).

https://doi.org/10.1016/j.bios.2020.112690
Received 22 July 2020; Received in revised form 26 September 2020; Accepted 4 October 2020
Available online 7 October 2020
0956-5663/© 2020 Elsevier B.V. All rights reserved.

conductors and amplifiers (Li et al., 2020b). However, the inherent fragility of the enzyme restricts the effectiveness of the enzyme system in practical operation (Bornscheuer et al., 2012), such as its vulnerability to surrounding fluctuations (Sheldon and Woodley, 2018) and its low tolerance to most organic solvents (Schmid et al., 2001) and small molecule inhibitors (Klibanov, 2001). Metal-organic frameworks (MOFs) have attracted extensive attention in separation (Lian et al., 2017), catalysis (Huo et al., 2015), sensing and drug delivery in past few years (Doonan et al., 2017), due to its merits of high surface area and porosity (Pang et al., 2018), diversity and versatile framework compositions (Liang et al., 2015). MOFs have been used as exoskeletons to protect vulnerable biological macromolecules including enzymes (Hu et al., 2018), DNA, and even viruses in very recent works (Feng et al., 2019). Chen. et al. encapsulated glucose oxidase (GOx) and horse radish peroxidase (HRP) in ZIF-8 NMOFs (Chen et al., 2018). Song et al. encapsulated multiple enzyme and DNA in ZIF-8 crystal (Song et al., 2019). Our research group encapsulated laccase (LAC) into ZIF-8 with unprecedented stability in previous work (Li et al., 2020a). This novel embedding strategy is not only capable of improving the stability of encapsulation enzymes by structural constraints, but also allows the selective transfer via the accessible microporous network (Zhang et al., 2019). Such symbiotic enhancement endows enzymes with great potential in biocatalysis (Zhang et al., 2018), biosensors and drug carrier for cancer (Zhou et al., 2019).

Flexible electronics hold great prospect in biomedical applications, such as artificial muscle, implantable biodevices (Gwon et al., 2014), skin sensors and electronic skin (Yousaf et al., 2016). Flexible electrodes as key link require strong mechanical property (Wen et al., 2016), precise integration of redox moieties and flexible independence (Li et al., 2014). Nevertheless, integrating the aforesaid merits within a single electrode is still a challenge (Wang et al., 2017). Cellulose/carbon nanotubes (CNTs)-based platforms have been considered ideal flexible electrode materials for lithium batteries (Moghadam et al., 2015), fuel cells (Pan et al., 2016), and sensors in recent years (Yin et al., 2016). Cellulose is a biocompatible linear polysaccharide (Kim et al., 2018), and the characteristics of sustainability, intrinsic flexibility and high strength (Ullah et al., 2016) make cellulose conducive to the long-term stability of the sensor in vitro and in vivo (Kim et al., 2019). Moreover, cellulose can utilize as inherent electrolyte reservoir benefit by hydrophilicity (Mulyadi et al., 2017). The hierarchical porous structure capable of transferring the diffuse ions in electrolytes and electrolytes to electrochemical active materials (Tedeschi et al., 2018). CNTs have been acted as conductive nanowires to effectively promote direct electron transfer (DET) because of its advantages of high surface area (Zhang and Zhao, 2009), high conductivity (Liu et al., 2014), tunable functional surface and nanoscale size (Choudhary et al., 2017). Xu. et al. designed a foldable electrodes based on nanocellulose and carbon nanotubes for energy storage devices (Xu et al., 2018). Our research group reported a novel single-enzymatic biofuel cell utilizing bacterial cellulose/CNTs-based highly flexible conductive electrode (Li et al., 2020b).

Gold nanoparticles (AuNPs) are noble metal nanoparticles with great potential to be widely used in food safety detection (Daniel and Astruc, 2004), biological analysis and catalysis due to its excellent biocompatibility (Jain et al., 2008), chemical inertness and abundant electronic and optical properties (Hu et al., 2006). Importantly, benefit by its chemical inertness and low toxicity (Jin, 2012), AuNPs was used to connect biomolecules (Oliveira et al., 2009) for biosensors based on DET between active center and electrode (Lim et al., 2017). In this work, we explored the in-situ growth of ZIF-8 on electrospun cellulose acetate (CA) nanofiber membranes with encapsulating LAC and glucose oxidase (GOx) into ZIF-8 during the growth process, respectively. Moreover, the highly flexible conductive electrodes were prepared by adsorbing multiwalled carbon nanotubes (MWCNTs) and AuNPs step by step on CA/ZIF-8@enzyme membranes. Furthermore, we established a platform of self-powered biosensor to monitor glucose utilizing nanostructured electrodes of CA/ZIF-8@GOx/MWCNTs/Au and CA/ZIF-8@LAC/MWCNTs/Au as anode and cathode, respectively. The as-proposed self-powered glucose sensors demonstrated a significant enhancement of long-term stability with continuous work of up to 15 h. The strategy of in-situ growth of MOFs on cellulose nanofiber with encapsulating enzyme into MOFs in the meantime, provides an innovative approach to establish various stable and reliable EBFC-based biosensors.

2. Experimental

2.1. Materials

Cellulose acetate (CA, M_w = 840,000 Da) was provided by Nantong Cellulose Fibers Co., Ltd. (Nantong, China). LAC from Ganoderma lucidum, GOx from Aspergillus niger and D-glucose were purchased from Sigma-Aldrich (St. Louis, MO). Multiwalled carbon nanotubes (water dispersions, 10 wt%) were supplied from Nanjing XFNANO Materials Tech Co., Ltd. (Nanjing, China). Besides, Acetone (CH_3COCH_3), N,N-dimethylacetamide (DMAC), 2-methylimidazole (2-MIM), zinc nitrate ($Zn(NO_3)_2{\cdot}6H_2O$), fluorescein isothiocyanate (FITC), hydrochloroauric acid trihydrate ($HAuCl_4{\cdot}3H_2O$, 99.9%) and sodium citrate ($Na_3C_6H_5O_7{\cdot}2H_2O$) were purchased from Aladdin Chemical Reagent Co. Ltd (Shanghai, China) and used without further purification.

2.2. Preparation of CA nanofiber membrane

CA nanofiber membrane was prepared by electrospinning. 12 wt% of CA spinning solution which used the mixture of acetone and DMAC (volume ratio is 3:2) as solvent was stirring for 8 h. The CA nanofibers were obtained by electrospinning technique through the self-made electrospinning device. The electrospun CA nanofiber membrane was then dried at 45 °C for future usage.

2.3. Synthesis of CA/ZIF-8@enzyme

Scheme S1 illustrates the synthesis mechanism of CA/ZIF-8@enzyme/MWCNTs/Au electrode. Specifically, 80 mL zinc nitrate solution containing 10 mL enzyme was stirred for 30 min. Then, CA nanofiber membrane was immersed in the mixture solution for 12 h. After washing by PBS solution, the membrane was transferred to 80 mL of 2-MIM solution without stirring for 1 d. Finally, the obtained CA/ZIF-8@enzyme membrane was washed thoroughly to remove the impurities attached to the surface.

2.4. Preparation of CA/ZIF-8@enzyme/MWCNTs/Au electrode

The obtained CA/ZIF-8@enzyme was firstly soaked in CNTs dispersions for a few seconds and then dried at 50 °C. Followed through adsorption with AuNPs solution, the CA/ZIF-8@enzyme/MWCNTs/Au was successfully prepared (Fig. S1). AuNPs were synthesized in one step. $HAuCl_4$ (1.0 mM, 50 mL) solution was heated to 110 °C in a 100 mL Erlenmeyer flask. The sodium citrate solution (1%, 10 mL) was then added drop by drop and heated continuously for 10 min. The AuNPs were successfully synthesized as the reaction solution changed from bright yellow to pink purple and stored for future usage. The synthesized AuNPs were examined by TEM (Figs. S2 and S3) and UV–vis spectrophotometer while the highest absorption wavelength was located at 524 nm (Fig. S4).

2.5. Materials characterization

Surface morphologies were characterized by FE-SEM. Chemical compositions were examined by EDS. The crystal morphologies of the samples were measured by XRD and Raman microscope (Renishaw RM3000, Germany) with a 533 laser source. The enzyme in CA/ZIF-8@enzyme was located by Confocal Laser Scanning Microscopy

(CLSM, TCS SP8, Germany), while enzyme was labeled by FITC with excitation at 488 nm and the fluorescence signal was collected in a window from 495 to 545 nm (Fig. S5). Detailed characterization is provided in the supporting material.

2.6. Electrochemical measurement

Herein, we established a simple EBFC-based self-powered biosensor to monitor glucose concentration (Scheme 1) and the photo image of as-proposed self-powered biosensor is shown in Fig. S6. A Nafion (5 wt%) membrane was used to separate the dual-chamber biosensor which was made by two reagent bottles. As-prepared CA/ZIF-8@GOx/MWCNTs/Au and CA/ZIF-8@LAC/MWCNTs/Au were used as anode and cathode, respectively.

3. Results and discussion

3.1. Morphology analysis

The morphologies of CA, CA/ZIF-8@enzyme, CA/ZIF-8@enzyme/MWCNTs and CA/ZIF-8@enzyme/MWCNTs/Au are shown in Fig. 1. As-received CA nanofiber membrane (Fig. 1a) are found to have a three-dimensional network structure and smooth surface, which provides a transmission path for oxygen. The inset image of Fig. 1a shows the average diameter of CA nanofiber is about 233 nm. The SEM image shown in Fig. 1b confirms that CA/ZIF-8@enzyme nanofiber membrane is constituted by CA and ZIF-8 crystal. Besides, ZIF-8 crystal (≈1.2 μm) is threaded by crystalline CA nanofiber, leading to a unique string-beaded morphology with a diameter of 1.5 μm. After combined with MWCNTs, the CA/ZIF-8@enzyme/MWCNTs nanofiber membrane (Fig. 1c) with high-quality porous structure reaches a diameter of about 3 μm, forming a denser hierarchical porous structure that facilitates ion transportation and electrolyte penetration. Moreover, the SEM image of CA/ZIF-8@enzyme (Fig. S7) at a higher magnification (× 5.0 k) shows the clearly boundaries and corners while the boundaries and corners were covered by MWCNTs on CA/ZIF-8@enzyme/MWCNTs (Fig. S8) membrane. Fig. 1d shows the familiar morphology with CA/ZIF-8@enzyme/MWCNTs nanofiber membrane after being adsorbed with AuNPs, and the inset image reveals the good hydrophilicity while the static water contact angle of CA/ZIF-8@enzyme/MWCNTs/Au is 48.0°, which benefits for electrolyte penetration. Furthermore, in order to investigate the distribution of ZIF-8 and AuNPs throughout the composite membrane, SEM-EDS analysis is presented in Fig. 2a, it can effortlessly reveal the successfully overlaid CA surface by ZIF-8 (Fig. S9), MWCNTs (Fig. S10) and AuNPs. The elements' concentrations of C, O, N, Zn and Au on CA/ZIF-8@enzyme/MWCNTs/Au membrane are verified at about 61.89, 5.82, 15.63, 14.33 and 2.33 wt%, respectively (Fig. S11).

3.2. XRD, Raman and TG analysis

Fig. 2b shows the XRD patterns for acquiring the variations of crystal structure on each sample. There is no significant peak on CA nanofiber membrane, indicating that the CA polymer exhibits characteristic of amorphous. After self-assembled of ZIF-8@enzyme on the CA nanofibers, several diffraction peaks are appeared at 7.8°, 10.9°, 13.1°, 15.1°, 16.8°, 18.4°, 24.8° and 26.9° on CA/ZIF-8@enzyme nanofiber membrane, which are consistent with the ZIF-8 and CA/ZIF-8 peaks in previous report (Fig. S12) (Li et al., 2019). The XRD pattern of CA/ZIF-8@enzyme/MWCNTs shows the graphite (002) plane and (101) crystal plane at 26.6° and 43.3°, respectively (Li et al., 2020b). With covered by the AuNPs, the CA/ZIF-8@enzyme/MWCNTs/Au composite membrane depicts several peaks centered at 2θ of 38.6°, 44.7° and 78.4°, corresponding to the diffraction of (111), (200) and (311) crystal planes of AuNPs, respectively (Hu et al., 2006).

The Raman spectra shown in Fig. Fig. S13 confirm the embedding of MWCNTs and AuNPs on CA/ZIF-8@enzyme/MWCNTs/Au composite membrane. As can be seen, the spectra show three leading characteristic peaks of carbon structures D peak, G peak and 2D peak. G peak is caused by the scattering of sp^2 bonded carbon atoms in the graphite cluster at 1580 cm^{-1} (Tadepalli et al., 2018) while the scattering of the disordered graphite carbon cluster forms the D-peak, which is centered at 1350 cm^{-1}. The third peak (2D peak) at 2701 cm^{-1} benefits from the highest optical branched-phonon boundary near k point at the Brillouin zone boundary (Yang et al., 2020). These three peaks above are significantly enhanced after the adsorption with AuNPs on the surface. This is due to the significant enhancement effect of AuNPs on Raman spectra (Sun et al., 2019b).

TG analysis is a typical method to evaluate the thermal stability of composite nanofiber membrane, and the results are shown in Fig. S14. CA is degraded in three steps. From 30 to 100 °C, the first step is caused by the evaporation of residual absorbed water, whereas the followed steps of 100–300 °C and 300–550 °C represent the degradation of cellulose network typically. The final weight losses of CA, CA/ZIF-8@enzyme, CA/ZIF-8@enzyme/MWCNTs and CA/ZIF-8@enzyme/MWCNTs/Au are 92 wt%, 75 wt%, 58 wt% and 46 wt%, respectively. The result shows the gradual enhancement of thermal stability with the addition of ZIF-8@enzyme, MWCNTs and Au step by step on composite nanofiber membrane. This is due to their coating on the surface and the presence of hydrogen bonds can improve the thermal properties of cellulose chains (Pan et al., 2011).

3.3. BET, XPS and mechanical properties

The BET curves of CA, CA/ZIF-8@enzyme and CA/ZIF-8@enzyme/MWCNTs/Au shown in Fig. 2c are typical H4 hysteresis loops, which reveal the mesoporous structures of composite membranes. The BET surface area of CA (9.879 $m^2 g^{-1}$) is consistent with average level of the

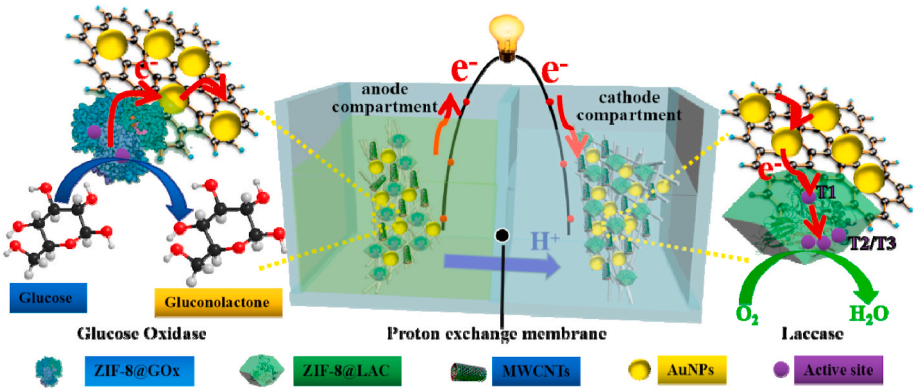

Scheme 1. Schematic of the EBFC-based self-powered glucose biosensor.

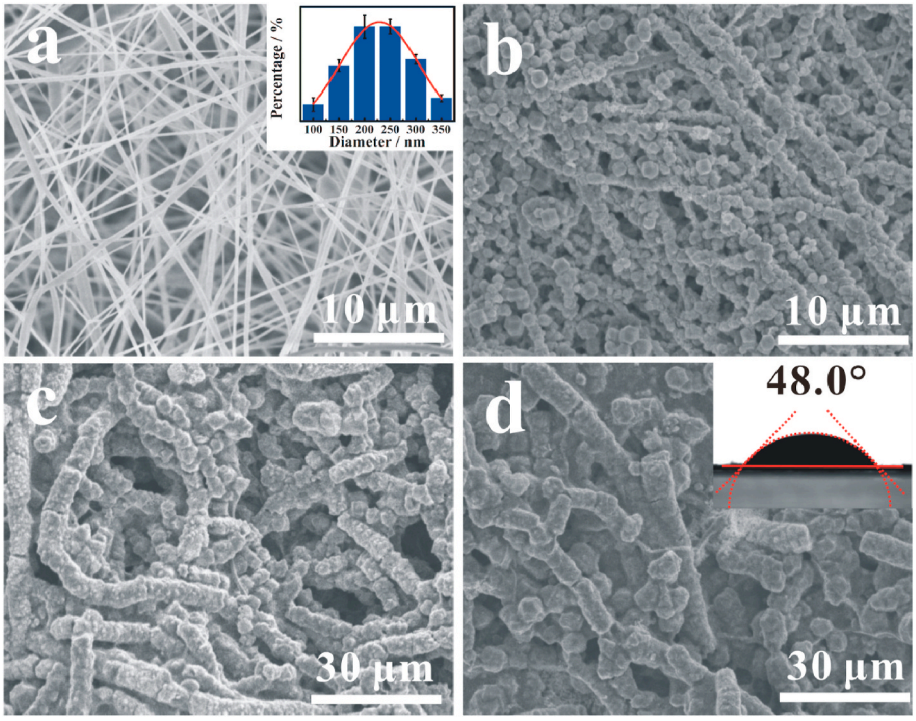

Fig. 1. FE-SEM images of (a) CA (with inset showing average size distribution of pure CA), (b) CA/ZIF-8@enzyme, (c) CA/ZIF-8@enzyme/MWCNTs and (d) CA/ZIF-8@enzyme/MWCNTs/Au (with inset showing the static water contact angle).

nanofiber while the CA/ZIF-8@enzyme exhibits ultra-high level of 163.730 m^2 g^{-1}, which is attribute to the porous structure and high absorption capacity of ZIF-8 crystal. In the process of in addition with MWCNTs and AuNPs, the composite membranes were immersed into water solution for several hours, which leading the swelling of CA nanofiber. This phenomenon may cause the damage of ZIF-8 on CA nanofiber and clog of external pores on ZIF-8, resulting in a significant reduction in the BET surface area of the CA/ZIF-8@enzyme/MWCNTs (102.325 m^2 g^{-1}) and CA/ZIF-8@enzyme/MWCNTs/Au (99.356 m^2 g^{-1}) membranes.

Figure S15 exhibits the typical tensile stress-strain curves of CA, CA/ZIF-8@enzyme, CA/ZIF-8@enzyme/MWCNTs and CA/ZIF-8@enzyme/MWCNTs/Au membranes. The results reveal the higher breaking stress of CA/ZIF-8@enzyme at 6.86 MPa while the pure CA membrane possesses a lower breaking strength at 5.34 MPa. This phenomenon could be ascribed to the enhancement of ZIF-8 on the membrane. After the absorption of MWCNTs, the mechanical properties of CA/ZIF-8@enzyme/MWCNTs depict significant increase, and it is easy to explain because several references have proved the enhancement of mechanical properties by MWCNTs. The decrease in mechanical strength of CA/ZIF-8@enzyme/MWCNTs/Au may be due to the swelling of CA nanofiber in AuNPs solution since it is well-known that the cellulose will swell while immersed into water solution.

X-ray test analyzed the elementary composition and electronic structure of C, O, N, Zn and Au on CA/ZIF-8@enzyme/MWCNTs/Au electrode, and the spectra are depicted in Fig. S16. In the spectra of the samples after in-situ growth with ZIF-8@enzyme (i.e. CA/ZIF-8@enzyme, CA/ZIF-8@enzym/MWCNTs and CA/ZIF-8@enzyme/MWCNTs/Au), N1s spectrum is significant centered at 398.3 eV (Figs. S16a and d). Whereas the Zn 2p atoms show two peaks of $2p_{3/2}$ and $2p_{1/2}$ located at 1021.9 and 1044.9 eV (Fig. S16e), which confirms the successful self-assemble of ZIF-8@enzyme on the nanofibers. Moreover, the fitted Au 4f peaks of CA/ZIF-8@enzyme/MWCNTs/Au nanofiber membrane consist of Au $4f_{5/2}$ and Au $4f_{7/2}$ at 87.1 and 83.5 eV (Fig. S16f), and it is contributed by the surface adsorption of AuNPs.

3.4. FV, FTIR and CLSM analysis

Fluorescence spectroscopy was used to measure the fluorescence emitted by phenylalanine, tryptophan and tyrosine in enzyme molecules to acquiring the tertiary structure changes of the enzyme. Due to the low fluorescence quantum yield of phenylalanine and weak fluorescence of tyrosine, fluorescence spectroscopy test usually select the fluorescence of tryptophan to analyze the enzyme structure while the fluorescence emission products of tryptophan derivatives (Trp −14, −142, −182, −185, −276 and −302) are sensitive to the environment, whether the enzyme residues are buried inside or exposed to the solvent. As shown in Fig. 3a, CA/ZIF-8@GOx and CA/ZIF-8@LAC exhibits the totally similar fluorescence spectra with the free GOx (λ_{max} = 329 nm) and LAC (λ_{max} = 332 nm) (Liang et al., 2019), revealing the successful immobilization of enzyme by CA/ZIF-8 membrane. Moreover, these dates also indicate that the enzyme structure shows no disturbance while it is encapsulated inside of CA/ZIF-8 membrane.

Fig. 3b exhibits the FTIR spectra of obtained membranes. The pure CA depicts several absorptions at 1741, 1373 and 1226 cm^{-1}, corresponding to the characteristic band of C═O, C–O and C–H of acetyl group (CHCOO), respectively. Moreover, the bands located in 1038 cm^{-1} is caused by hydroxyl ring of cellulose ether. After the in-situ growth of ZIF-8 crystal, several new bands appear on the CA/ZIF-8 spectrum. Specifically, the out-of-plane blending on 2-MIM depicts two new bands at 690 and 757 cm^{-1}, and the characteristic bands of in-plane bending on 2-MIM ring are centered between 845 and 1310 cm^{-1}. Meanwhile, the aliphatic and aromatic C–H stretch of 2-MIM corresponds to a new band at 2900 cm^{-1}. The spectrum of CA/ZIF-8@GOx exhibits two additional bands at 1644 and 1537 cm^{-1}, which is attributed to amide-I and amide-II groups of GOx molecules, respectively. Moreover, amido-I band on the spectrum of CA/ZIF-8@LAC that located in 1641 cm^{-1} is attributed to the C–N and N–H on LAC molecules, in addition, another sharp peak centered at 3432 cm^{-1} is also caused by LAC of O–H stretching. Nevertheless, these two bands move to the higher wavenumbers while they are centered at 1645 cm^{-1} and 3327 cm^{-1} on the pure LAC, which may be caused by the vibrations of amide

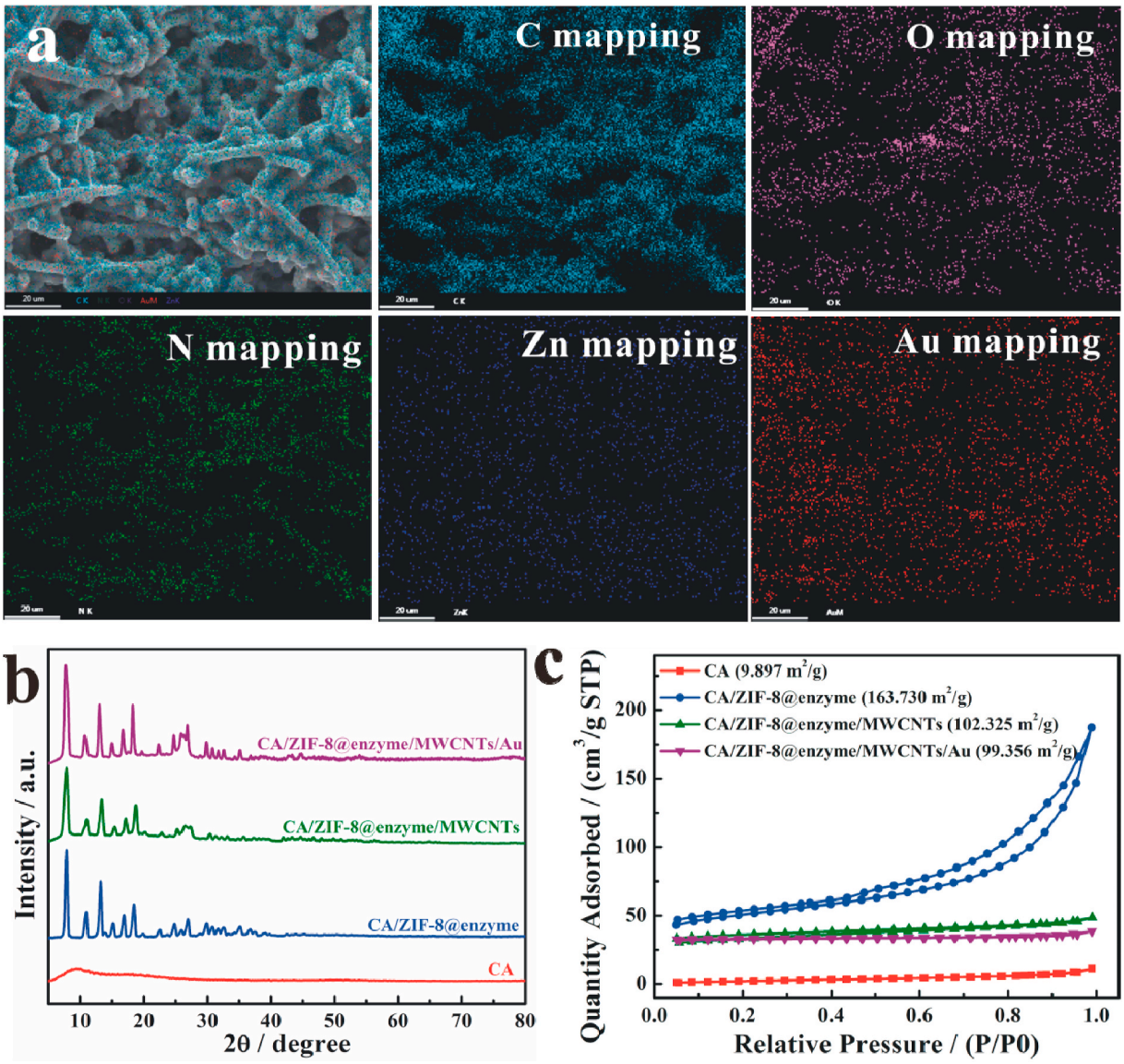

Fig. 2. (a) SEM-EDS elemental mapping images of CA/ZIF-8@enzyme/MWCNTs/Au electrode; (b) XRD patterns and (c) BET analysis of as-prepared samples.

in the immobilization process (Patil and Yadav, 2018).

In order to further explore the spatial distribution of enzyme on the CA/ZIF-8 nanofiber membranes, CLSM results are shown in Fig. 3c, d and Fig. S17. The two images show almost identical results to indicate that the enzyme is distributed throughout CA/ZIF-8@enzyme, not only encapsulated in ZIF-8 crystals, but also on the CA nanofiber membranes. Moreover, the inset images of Fig. 3c and d clearly show the homogeneous distribution of enzyme molecules throughout ZIF-8, verifying the feasibility of enzyme encapsulation strategy.

3.5. Electrochemical behavior

The electrochemical properties of CA/ZIF-8@enzyme/MWCNTs/Au electrodes were measured by cyclic voltammetry (CV). In Fig. 4a, a pair of significant redox peaks (~0.39 v and ~0.51 v) appears as expected in references on the CV curve of the CA/ZIF-8@LAC/MWCNTs/Au, which is caused by the redox reaction of T1 Cu active center to the electrode surface through the MWCNTs and AuNPs. In addition, with the increase in the scanning rate, the current of cathode shifts to more progressive values for redox reactions. According to the CV test of the cathode, we explored the surface-controlled process by establishing a curve between current and scanning rate, and the generated linear relationship (Fig. 4b) reveals the excellent scaling phenomenon of diffusion control system in the process of redox reaction. Importantly, the coupling of LAC and cathode is demonstrated and settles a theoretical foundation for electrochemical kinetics.

As shown in Fig. 4c, the electrochemical performance of anode exhibits a pair of redox peaks (~0.30 v and ~0.43 v) caused by the redox reaction of the anode enzyme (GOx molecules). As expected, the same phenomenon with the biocathode is found while the scan rate is increased from 50 to 300 mV/s. Fig. 4d exhibits a similar linear relationship between the oxidation and reduction currents with the increased scan rate, and it presents a good correlation while the R^2 of i_{pa} and i_{pc} are 0.991 and 0.997, respectively. The good coupling between GOx and anode is also demonstrated and the process is therefore surface-controlled by the CA/ZIF-8@GOx/MWCNTs/Au electrode.

3.6. Self-powered biosensor performance

Electrochemical impedance spectroscopy (EIS) was applied to characterize the resistance of electron in the process of BFC operation, the resulted impedance spectra are shown in Fig. 5a. The charge transfer

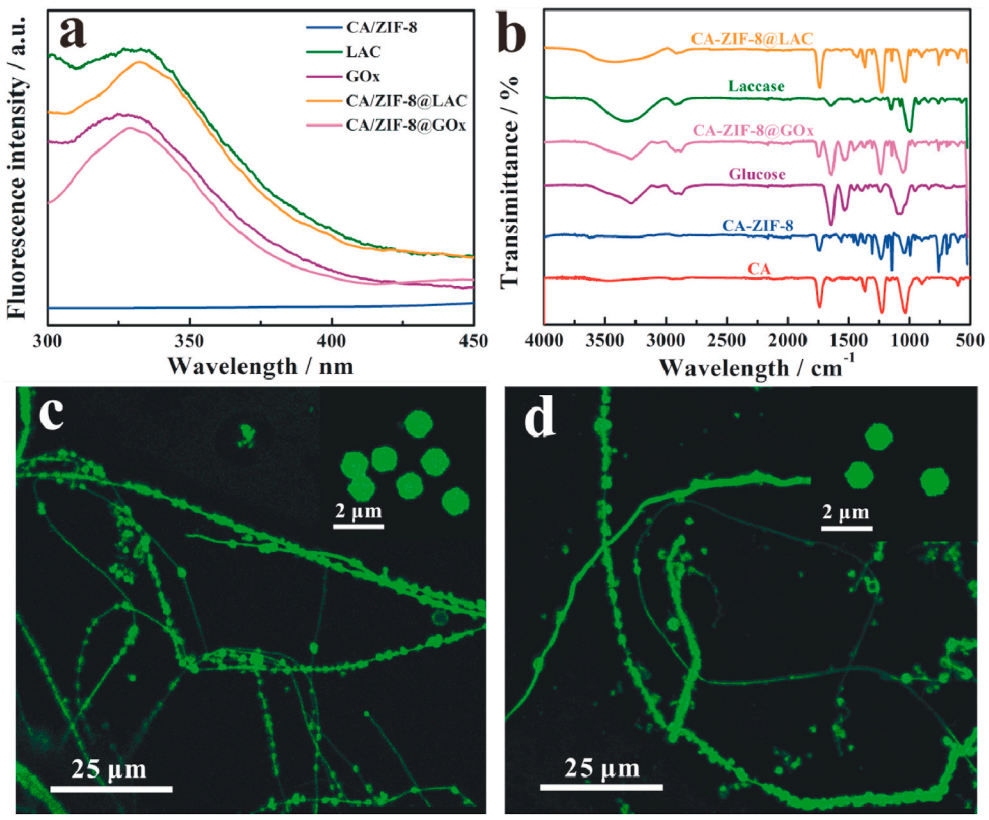

Fig. 3. (a) Fluorescence spectroscopy; (b) FT-IR spectra; CLSM images of (c) CA/ZIF-8@LAC and (d) CA/ZIF-8@GOx (with inset showing the CLSM images of individual ZIF-8@LAC and ZIF-8@GOx).

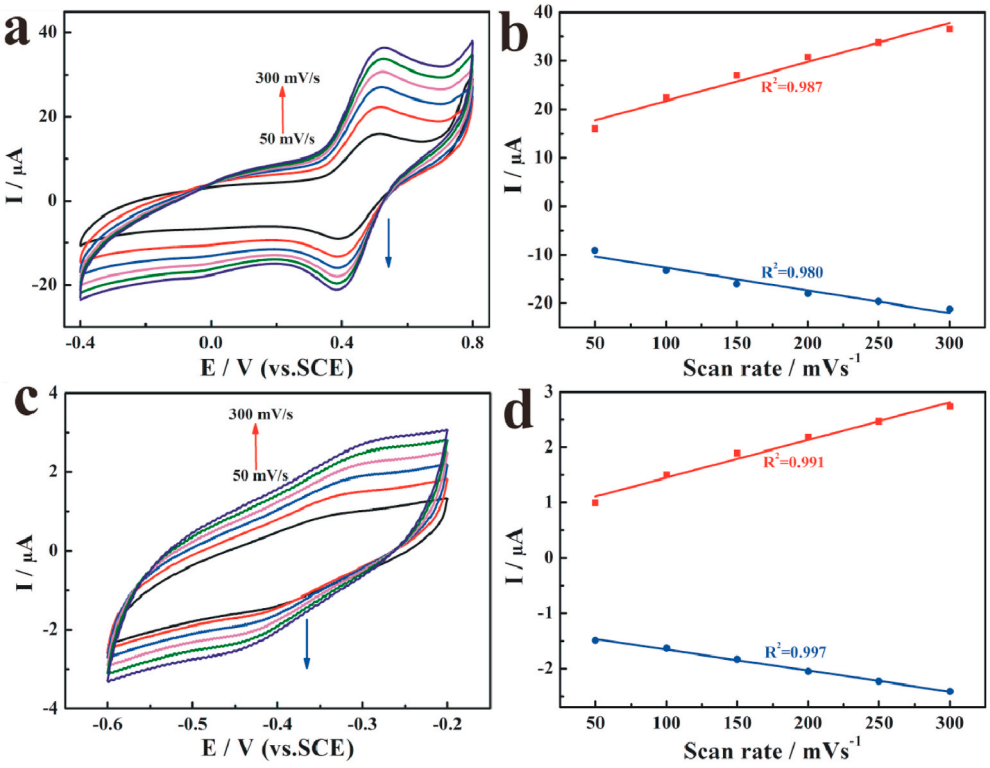

Fig. 4. Cyclic voltammograms of (a) CA/ZIF-8@LAC/MWCNTs/Au electrode and (c) CA/ZIF-8@GOx/MWCNTs/Au electrode at scan rates of 50–300 mV/s; Oxidation and reduction peak currents vs. the scan rates of each electrode (b and d).

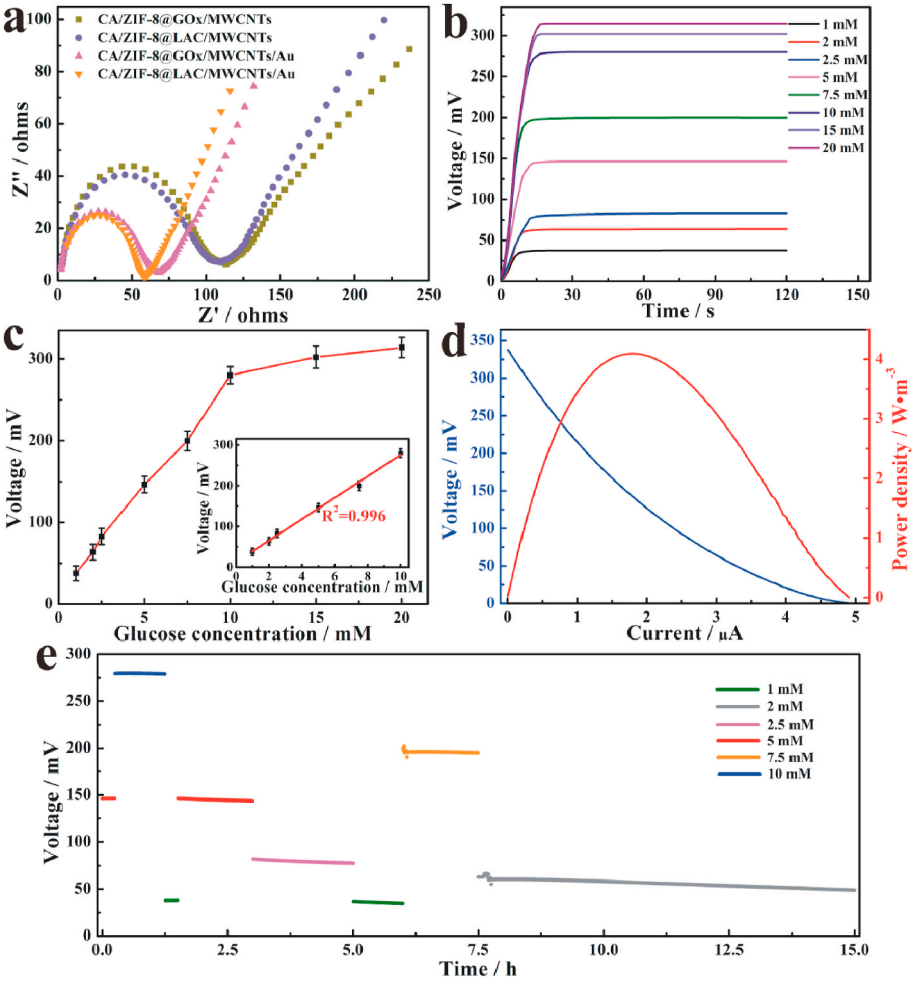

Fig. 5. Performance evaluation of as-proposed self-powered glucose sensor. (a) Nyquist plots from EIS measurements CA/ZIF-8@enzyme/MWCNTs and CA/ZIF-8@enzyme/MWCNTs/Au; (b) The E^{OCP} responses of self-powered glucose sensor based on nanostructured CA/ZIF-8@enzyme/MWCNTs/Au electrodes; (c) Sensitivity of self-powered glucose sensor with inset image of the linear relationship of E^{OCP} vs the concentration of glucose; (d) Power curves and polarization curves of the self-powered glucose sensor; (e) 15 h long-term measurement of the as-proposed self-powered glucose sensor.

resistance (R_{ct}) of CA/ZIF-8@enzyme/MWCNTs electrodes shows remarkably the increase compared to CA/ZIF-8/MWCNTs composite membranes, which is caused by the successful immobilization of enzyme (LAC and GOx). As-fabricated electrodes with lower R_{ct} exhibit a broad prospect in sensor application after being modified with AuNPs, and this is attributed to the excellent electrical conductivity of the AuNPs.

A self-powered sensor was established by coupling the CA/ZIF-8@enzyme/MWCNTs electrodes under the optimal experimental conditions. As expected, the variation of E^{OCP} was closely related to glucose concentration. In the range of 1–20 mM, E^{OCP} gradually increased with the elevated substrate concentration, but the change was slight after 10 mM(Fig. 5b), and the photo image of E^{OCP} for as-proposed biosensor under 10 mM glucose is shown in Fig. S18. Furthermore, the effective work of as-proposed self-powered glucose biosensor was proved while an excellent linear relationship between E^{OCP} and glucose concentration was fitted (Fig. 5c) from 1 to 10 mM. The linear equation is defined as $E^{OCP} = 26.346c+12.438$ ($R^2 = 0.996$) with an outstanding detection limit of 5.347 μM based on S/N = 3. Additionally, Fig. 5d exhibits the E^{OCP} curves and polarization curves under the condition of 10 mM glucose anolyte.

Long-term stability is a critical bottleneck for self-powered biosensor, particularly for non-invasive biosensors, continuous detection of up to 15 h in this work are rare. It is verified that the sensor is capable of producing the same level of E^{OCP} signal with refreshed substrate, which suggests that the sensitivity of the sensor is well preserved. This is mainly due to the adequate protection of MOF encapsulation enzyme strategy in the designed nanostructures. However, the reduction of E^{OCP} with the extension of working time can still be observed in Fig. 5e, which is a natural phenomenon, mainly due to the decrease of glucose concentration in the local environment and the loss of enzyme activity immobilized on CA nanofiber in the long-term measurement. In addition, the structure of as-proposed electrode (Fig. S19) shows no obvious change after 15 h.

4. Conclusions

The exploration of reliable long-term and real-time sensors to monitor human physiological conditions is of great significance for the increasingly ageing population (Lin et al., 2019b). Herein, we successfully encapsulated enzyme into ZIF-8 in the process of in-situ growth ZIF-8 on electrospun CA nanofiber membranes, and the CA/ZIF-8@enzyme/MWCNTs/Au membranes were utilized as highly flexible electrodes for self-powered glucose biosensor. Meanwhile, the as-proposed glucose biosensor held excellent long-term stability in continues works of up to 15 h. As-proposed biosensor came up with a very meaningful strategy for future population research on the correlation between glucose concentration in human sweat and physiological state.

Notes

There are no conflicts to declare.

CRediT authorship contribution statement

Xin Li: Data curation, Investigation, Writing - original draft, Writing - review & editing. **Quan Feng:** Investigation, Writing - review & editing. **Keyu Lu:** Data curation, Formal analysis. **Jieyu Huang:** Investigation. **Yanan Zhang:** Investigation. **Yutong Hou:** Investigation. **Hui Qiao:** Investigation, Writing - review & editing. **Dawei Li:** Conceptualization, Project administration, Investigation, Writing - review & editing. **Qufu Wei:** Project administration, Conceptualization, Data curation, Investigation, Writing - review & editing.

Declaration of competing interest

The authors declare that they have no known competing financial interests or personal relationships that could have appeared to influence the work reported in this paper.

Acknowledgements

This research was financially supported by National Key R&D Program of China (2017YFB0309100), Key Laboratory of Eco-textiles, Ministry of Education-supported by the Fundamental Research Funds for the Central Universities (JUSRP52007A), the national first-class discipline program of Light Industry Technology and Engineering (LITE 2018-21), the Natural Science Foundation of Jiangsu Province (BK20180628), the National Natural Science Foundation of China (51803078), the China Postdoctoral Science Foundation (2018T110442 and 2017M610296), 111 Project (B17021).

Appendix A. Supplementary data

Supplementary data to this article can be found online at https://doi.org/10.1016/j.bios.2020.112690.

References

Barton, S.C., Gallaway, J., Atanassov, P., 2004. Enzymatic biofuel cells for Implantable and microscale devices. Chem. Rev. 104, 4867–4886.
Bornscheuer, U.T., Huisman, G.W., Kazlauskas, R.J., Lutz, S., Moore, J.C., Robins, K., 2012. Engineering the third wave of biocatalysis. Nature 485, 185–194.
Chen, W.-H., Vazquez-Gonzalez, M., Zoabi, A., Abu-Reziq, R., Willner, I., 2018. Biocatalytic cascades driven by enzymes encapsulated in metal-organic framework nanoparticles. Nat. Catal. 1, 689–695.
Chen, Y., Ji, W., Yan, K., Gao, J., Zhang, J., 2019. Fuel cell-based self-powered electrochemical sensors for biochemical detection. Nanomater. Energy 61, 173–193.
Chen, G., Kou, X., Huang, S., Tong, L., Shen, Y., Zhu, W., Zhu, F., Ouyang, G., 2020. Modulating the biofunctionality of metal-organic framework-encapsulated enzymes through controllable embedding patterns. Angew. Chem. Int. Ed. 59, 2867–2874.
Choudhary, N., Li, C., Moore, J., Nagaiah, N., Zhai, L., Jung, Y., Thomas, J., 2017. Asymmetric supercapacitor electrodes and devices. Adv. Mater. 29, 1605336.
Daniel, M.C., Astruc, D., 2004. Gold nanoparticles: assembly, supramolecular chemistry, quantum-size-related properties, and applications toward biology, catalysis, and nanotechnology. Chem. Rev. 104, 293–346.
Doonan, C., Ricco, R., Liang, K., Bradshaw, D., Falcaro, P., 2017. Metal-organic frameworks at the biointerface: synthetic strategies and applications. Accounts Chem. Res. 50, 1423–1432.
Fan, Y.-J., Huang, M.-Z., Hsiao, Y.-C., Huang, Y.-W., Deng, C.-Z., Yeh, C., Husain, R.A., Lin, Z.-H., 2020. Enhancing the sensitivity of portable biosensors based on self-powered ion concentration polarization and electrical kinetic trapping. Nanomater. Energy 69, 104407.
Feng, Y., Wang, H., Zhang, S., Zhao, Y., Gao, J., Zheng, Y., Zhao, P., Zhang, Z., Zaworotko, M.J., Cheng, P., Ma, S., Chen, Y., 2019. Antibodies@MOFs: an in vitro protective coating for preparation and storage of biopharmaceuticals. Adv. Mater. 31, 1805148.
Gao, W., Emaminejad, S., Nyein, H.Y.Y., Challa, S., Chen, K., Peck, A., Fahad, H.M., Ota, H., Shiraki, H., Kiriya, D., Lien, D.-H., Brooks, G.A., Davis, R.W., Javey, A., 2016. Fully integrated wearable sensor arrays for multiplexed in situ perspiration analysis. Nature 529, 509.
Gwon, H., Hong, J., Kim, H., Seo, D.-H., Jeon, S., Kang, K., 2014. Recent progress on flexible lithium rechargeable batteries. Energy Environ. Sci. 7, 538–551.
Hu, M., Chen, J., Li, Z.-Y., Au, L., Hartland, G.V., Li, X., Marquez, M., Xia, Y., 2006. Gold nanostructures: engineering their plasmonic properties for biomedical applications. Chem. Soc. Rev. 35, 1084–1094.
Hu, Y., Dai, L., Liu, D., Du, W., Wang, Y., 2018. Progress & prospect of metal-organic frameworks (MOFs) for enzyme immobilization (enzyme/MOFs). Renew. Sustain. Energy Rev. 91, 793–801.
Huo, J., Aguilera-Sigalat, J., El-Hankari, S., Bradshaw, D., 2015. Magnetic MOF microreactors for recyclable size-selective biocatalysis. Chem. Sci. 6, 1938–1943.
Jain, P.K., Huang, X., El-Sayed, I.H., El-Sayed, M.A., 2008. Noble metals on the nanoscale: optical and photothermal properties and some applications in imaging, sensing, biology, and medicine. Accounts Chem. Res. 41, 1578–1586.
Jin, Y., 2012. Engineering plasmonic gold nanostructures and metamaterials for biosensing and nanomedicine. Adv. Mater. 24, 5153–5165.
Katz, E., Buckmann, A.F., Willner, I., 2001. Self-powered enzyme-based biosensors. J. Am. Chem. Soc. 123, 10752–10753.
Kim, I., Jeon, H., Kim, D., You, J., Kim, D., 2018. All-in-one cellulose based triboelectric nanogenerator for electronic paper using simple filtration process. Nanomater. Energy 53, 975–981.
Kim, K.O., Kim, G.J., Kim, J.H., 2019. A cellulose/beta-cyclodextrin nanofiber patch as a wearable epidermal glucose sensor. RSC Adv. 9, 22790–22794.
Klibanov, A.M., 2001. Improving enzymes by using them in organic solvents. Nature 409, 241–246.
Kwon, C.H., Ko, Y., Shin, D., Lee, S.W., Cho, J., 2019. Highly conductive electrocatalytic gold nanoparticle-assembled carbon fiber electrode for high-performance glucose-based biofuel cells. J. Mater. Chem. 7, 13495–13505.
Lee, H., Hong, Y.J., Baik, S., Hyeon, T., Kim, D.-H., 2018. Enzyme-based glucose sensor: from invasive to wearable device. Adv. Healthc. Mater. 7, 1701150.
Li, L., Wu, Z., Yuan, S., Zhang, X.-B., 2014. Advances and challenges for flexible energy storage and conversion devices and systems. Energy Environ. Sci. 7, 2101–2122.
Li, N., Zhou, L., Jin, X., Owens, G., Chen, Z., 2019. Simultaneous removal of tetracycline and oxytetracycline antibiotics from wastewater using a ZIF-8 metal organic-framework. J. Hazard Mater. 366, 563–572.
Li, X., Li, D., Zhang, Y., Lv, P., Feng, Q., Wei, Q., 2020a. Encapsulation of enzyme by metal-organic framework for single-enzymatic biofuel cell-based self-powered biosensor. Nanomater. Energy 68, 104308.
Li, X., Lv, P., Yao, Y., Feng, Q., Mensah, A., Li, D., Wei, Q., 2020b. A novel single-enzymatic biofuel cell based on highly flexible conductive bacterial cellulose electrode utilizing pollutants as fuel. Chem. Eng. J. 379, 122316.
Lian, X., Fang, Y., Joseph, E., Wang, Q., Li, J., Banerjee, S., Lollar, C., Wang, X., Zhou, H.-C., 2017. Enzyme-MOF (metal-organic framework) composites. Chem. Soc. Rev. 46, 3386–3401.
Liang, K., Ricco, R., Doherty, C.M., Styles, M.J., Bell, S., Kirby, N., Mudie, S., Haylock, D., Hill, A.J., Doonan, C.J., Falcaro, P., 2015. Biomimetic mineralization of metal-organic frameworks as protective coatings for biomacromolecules. Nat. Commun. 6, 7240.
Liang, W., Xu, H., Carraro, F., Maddigan, N.K., Li, Q., Bell, S.G., Huang, D.M., Tarzia, A., Solomon, M.B., Amenitsch, H., Vaccari, L., Sumby, C.J., Falcaro, P., Doonan, C.J., 2019. Enhanced activity of enzymes encapsulated in hydrophilic metal-organic frameworks. J. Am. Chem. Soc. 141, 2348–2355.
Lim, G.-H., Kwak, S.S., Kwon, N., Kim, T., Kim, H., Kim, S.M., Kim, S.-W., Lim, B., 2017. Fully stretchable and highly durable triboelectric nanogenerators based on gold-nanosheet electrodes for self-powered human-motion detection. Nanomater. Energy 42, 300–306.
Lin, Y., Chen, J., Tavakoli, M.M., Gao, Y., Zhu, Y., Zhang, D., Kam, M., He, Z., Fan, Z., 2019a. Printable fabrication of a fully integrated and self-powered sensor system on plastic substrates. Adv. Mater. 31, 1804285.
Lin, Y., Bariya, M., Nyein, H.Y.Y., Kivimaki, L., Uusitalo, S., Jonsson, E., Ji, W., Yuan, Z., Happonen, T., Liedert, C., Hiltunen, J., Fan, Z., Javey, A., 2019b. Porous enzymatic membrane for nanotextured glucose sweat sensors with high stability toward reliable noninvasive health monitoring. Adv. Funct. Mater. 29, 1902521.
Lipani, L., Dupont, B.G.R., Doungmene, F., Marken, F., Tyrrell, R.M., Guy, R.H., Ilie, A., 2018. Non-invasive, transdermal, path-selective and specific glucose monitoring via a graphene-based platform. Nat. Nanotechnol. 13, 504.
Liu, T., Finn, L., Yu, M., Wang, H., Zhai, T., Lu, X., Tong, Y., Li, Y., 2014. Polyaniline and polypyrrole pseudocapacitor electrodes with excellent cycling stability. Nano Lett. 14, 2522–2527.
Lv, P., Zhou, H., Mensah, A., Feng, Q., Wang, D., Hu, X., Cai, Y., Lucia, L.A., Li, D., Wei, Q., 2018. A highly flexible self-powered biosensor for glucose detection by epitaxial deposition of gold nanoparticles on conductive bacterial cellulose. Chem. Eng. J. 351, 177–188.
Mahmoodi, N.M., Saffar-Dastgerdi, M.H., 2020. Clean Laccase immobilized nanobiocatalysts (graphene oxide-zeolite nanocomposites): from production to detailed biocatalytic degradation of organic pollutant. Appl. Catal. B Environ. 268, 118443.
Miyake, T., Haneda, K., Nagai, N., Yatagawa, Y., Onami, H., Yoshino, S., Abe, T., Nishizawa, M., 2011. Enzymatic biofuel cells designed for direct power generation from biofluids in living organisms. Energy Environ. Sci. 4, 5008–5012.
Moghadam, A.D., Omrani, E., Menezes, P.L., Rohatgi, P.K., 2015. Mechanical and tribological properties of self-lubricating metal matrix nanocomposites reinforced by carbon nanotubes (CNTs) and graphene-A review. Compos. B Eng. 77, 402–420.
Mulyadi, A., Zhang, Z., Dutzer, M., Liu, W., Deng, Y., 2017. Facile approach for synthesis of doped carbon electrocatalyst from cellulose nanofibrils toward high-performance metal-free oxygen reduction and hydrogen evolution. Nanomater. Energy 32, 336–346.
Nyein, H.Y.Y., Gao, W., Shahpar, Z., Emaminejad, S., Challa, S., Chen, K., Fahad, H.M., Tai, L.-C., Ota, H., Davis, R.W., Javey, A., 2016. A wearable electrochemical platform for noninvasive simultaneous monitoring of Ca^{2+} and pH. ACS Nano 10, 7216–7224.

Oliveira, R.L., Kiyohara, P.K., Rossi, L.M., 2009. Clean preparation of methyl esters in one-step oxidative esterification of primary alcohols catalyzed by supported gold nanoparticles. Green Chem. 11, 1366–1370.
Pan, Y., Liu, Y., Zeng, G., Zhao, L., Lai, Z., 2011. Rapid synthesis of zeolitic imidazolate framework-8 (ZIF-8) nanocrystals in an aqueous system. Chem. Commun. 47, 2071–2073.
Pan, Y., Lin, Y., Liu, Y., Liu, C., 2016. A novel CoP/MoS_2-CNTs hybrid catalyst with Pt-like activity for hydrogen evolution. Catal. Sci. Technol. 6, 1611–1615.
Pang, Y., Li, H., Farmakes, J., Xiao, F., Chen, B., Ma, S., Yang, Z., 2018. How do enzymes orient when trapped on metal-organic framework (MOF) surfaces? J. Am. Chem. Soc. 140, 16032–16036.
Park, J., Kim, J., Kim, S.-Y., Cheong, W.H., Jang, J., Park, Y.-G., Na, K., Kim, Y.-T., Heo, J.H., Lee, C.Y., Lee, J.H., Bien, F., Park, J.-U., 2018. Soft, smart contact lenses with integrations of wireless circuits, glucose sensors, and displays. Sci. Adv. 4, 9841.
Patil, P.D., Yadav, G.D., 2018. Rapid in situ encapsulation of laccase into metal-organic framework support (ZIF-8) under biocompatible conditions. Chemistry 3, 4669–4675.
Sakthivel, M., Ramaraj, S., Chen, S.-M., Chen, T.-W., Ho, K.-C., 2019. Transition-metal-Doped molybdenum diselenides with defects and abundant active sites for efficient performances of enzymatic biofuel cell and supercapacitor applications. ACS Appl. Mater. Interfaces 11, 18483–18493.
Schmid, A., Dordick, J.S., Hauer, B., Kiener, A., Wubbolts, M., Witholt, B., 2001. Industrial biocatalysis today and tomorrow. Nature 409, 258–268.
Sheldon, R.A., Woodley, J.M., 2018. Role of biocatalysis in sustainable chemistry. Chem. Rev. 118, 801–838.
Song, J., He, W., Shen, H., Zhou, Z., Li, M., Su, P., Yang, Y., 2019. Construction of multiple enzyme metal-organic frameworks biocatalyst via DNA scaffold: a promising strategy for enzyme encapsulation. Chem. Eng. J. 363, 174–182.
Sun, X., Zhang, H., Hao, S., Zhai, J., Dong, S., 2019a. A self-powered biosensor with a flake electrochromic display for electrochemical and colorimetric formaldehyde detection. ACS Sens. 4, 2631–2637.
Sun, H., Cong, S., Zheng, Z., Wang, Z., Chen, Z., Zhao, Z., 2019b. Metal-organic frameworks as surface enhanced Raman scattering substrates with high tailorability. J. Am. Chem. Soc. 141, 870–878.
Tadepalli, S., Yim, J., Cao, S., Wang, Z., Naik, R.R., Singamaneni, S., 2018. Metal-organic framework encapsulation for the preservation and photothermal enhancement of enzyme activity. Small 14, 1702382.
Tedeschi, G., Guzman-Puyol, S., Paul, U.C., Barthel, M.J., Goldoni, L., Caputo, G., Ceseracciu, L., Athanassiou, A., Heredia-Guerrero, J.A., 2018. Thermoplastic cellulose acetate oleate films with high barrier properties and ductile behaviour. Chem. Eng. J. 348, 840–849.
Ullah, H., Santos, H.A., Khan, T., 2016. Applications of bacterial cellulose in food, cosmetics and drug delivery. Cellulose 23, 2291–2314.
Wang, H.-G., Li, W., Liu, D.-P., Feng, X.-L., Wang, J., Yang, X.-Y., Zhang, X.-b., Zhu, Y., Zhang, Y., 2017. Flexible electrodes for sodium-ion batteries: recent progress and perspectives. Adv. Mater. 29, 1703012.
Wang, L.-L., Shao, H.-H., Wang, W.-J., Zhang, J.-R., Zhu, J.-J., 2018. Nitrogen-doped hollow carbon nanospheres for high-energy-density biofuel cells and self-powered sensing of microRNA-21 and microRNA-141. Nanomater. Energy 44, 95–102.
Wen, L., Li, F., Cheng, H.-M., 2016. Carbon nanotubes and graphene for flexible electrochemical energy storage: from materials to devices. Adv. Mater. 28, 4306–4337.
Xu, S., Qin, Y., Xu, C., Wei, Y., Yang, R., Wang, Z.L., 2010. Self-powered nanowire devices. Nat. Nanotechnol. 5, 366–373.
Xu, C., Kong, X., Zhou, S., Zheng, B., Huo, F., Stromme, M., 2018. Interweaving metal-organic framework- templated Co-Ni layered double hydroxide nanocages with nanocellulose and carbon nanotubes to make flexible and foldable electrodes for energy storage devices. J. Mater. Chem. 6, 24050–24057.
Yang, Y., Gao, W., 2019. Wearable and flexible electronics for continuous molecular monitoring. Chem. Soc. Rev. 48, 1465–1491.
Yang, Z., Qin, T., Niu, Y., Zhang, Y., Zhang, C., Li, P., Zhu, M., Jia, Y., Li, Q., 2020. Flexible visible-light-driven photoelectrochemical biosensor based on molecularly imprinted nanoparticle intercalation-modulated graphene fiber for ultrasensitive urea detection. Carbon 157, 457–465.
Yin, Y., Liu, X., Wei, X., Yu, R., Shui, J., 2016. Porous CNTs/Co composite derived from zeolitic imidazolate framework: a lightweight, ultrathin, and highly efficient electromagnetic wave absorber. ACS Appl. Mater. Interfaces 8, 34686–34698.
Yousaf, M., Shi, H.T.H., Wang, Y., Chen, Y., Ma, Z., Cao, A., Naguib, H.E., Han, R.P.S., 2016. Novel pliable electrodes for flexible electrochemical energy storage devices: recent progress and challenges. Adv. Energy Mater. 6, 1600490.
Zhang, L.L., Zhao, X.S., 2009. Carbon-based materials as supercapacitor electrodes. Chem. Soc. Rev. 38, 2520–2531.
Zhang, L., Wang, Z., Zhang, Y., Cao, F., Dong, K., Ren, J., Qu, X., 2018. Erythrocyte membrane cloaked metal-organic framework nanoparticle as biomimetic nanoreactor for starvation-activated colon cancer therapy. ACS Nano 12, 10201–10211.
Zhang, C., Zhang, L., Wu, W., Gao, F., Li, R.-Q., Song, W., Zhuang, Z.-N., Liu, C.-J., Zhang, X.-Z., 2019. Artificial super neutrophils for inflammation targeting and HClO generation against tumors and infections. Adv. Mater. 31, 1901179.
Zhou, D., Ni, J., Li, L., 2019. Self-supported multicomponent CPO-27 MOF nanoarrays as high-performance anode for lithium storage. Nanomater. Energy 57, 711–717.